

Rescue of mis-splicing of a common *SLC26A4* mutant associated with sensorineural hearing loss by antisense oligonucleotides

Pengchao Feng,^{1,2,9} Zhijiao Xu,^{3,4,5,9} Jialin Chen,^{1,2} Meizhen Liu,⁶ Yu Zhao,^{3,4,5} Daqi Wang,^{3,4,5} Lei Han,^{3,4,5,6,7} Li Wang,⁸ Bo Wan,^{1,2} Xingshun Xu,^{1,2} Dali Li,⁶ Yilai Shu,^{3,4,5} and Yimin Hua⁸

¹Department of Neurology and Suzhou Clinical Research Center of Neurological Disease, The Second Affiliated Hospital of Soochow University, 1055 Sanxiang Road, Suzhou 215004, China; ²Institute of Neuroscience, Soochow University, 199 Renai Road, Suzhou, Jiangsu 215123, China; ³ENT Institute and Department of Otorhinolaryngology, Eye & ENT Hospital, State Key Laboratory of Medical Neurobiology and MOE Frontiers Center for Brain Science, Fudan University, Shanghai 200031, China; ⁴Institutes of Biomedical Sciences, Fudan University, Shanghai 200032, China; ⁵NHC Key Laboratory of Hearing Medicine (Fudan University), Shanghai 200032, China; ⁶Shanghai Key Laboratory of Regulatory Biology, Institute of Biomedical Sciences and School of Life Sciences, East China Normal University, Shanghai 200241, China; ⁷Department of Otorhinolaryngology, The Second Affiliated Hospital, University of South China, Hengyang 421001, China; ⁸Jiangsu Key Laboratory for Molecular and Medical Biotechnology, College of Life Sciences, Nanjing Normal University, Nanjing 210023, China

A wide spectrum of *SLC26A4* mutations causes Pendred syndrome and enlarged vestibular aqueduct, both associated with sensorineural hearing loss (SNHL). A splice-site mutation, c.919-2A>G (A-2G), which is common in Asian populations, impairs the 3' splice site of intron 7, resulting in exon 8 skipping during pre-mRNA splicing and a subsequent frameshift that creates a premature termination codon in the following exon. Currently, there is no effective drug treatment for SNHL. For A-2G-triggered SNHL, molecules that correct mis-splicing of the mutant hold promise to treat the disease. Antisense oligonucleotides (ASOs) can promote exon inclusion when targeting specific splicing silencers. Here, we systematically screened a large number of ASOs in a minigene system and identified a few that markedly repressed exon 8 skipping. A lead ASO, which targets a heterogeneous nuclear ribonucleoprotein (hnRNP) A1/A2 intronic splicing silencer (ISS) in intron 8, promoted efficient exon 8 inclusion in cultured peripheral blood mononuclear cells derived from two homozygous patients. In a partially humanized *Slc26a4* A-2G mouse model, two subcutaneous injections of the ASO at 160 mg/kg significantly rescued exon 8 splicing in the liver. Our results demonstrate that the ISS-targeting ASO has therapeutic potential to treat genetic hearing loss caused by the A-2G mutation in *SLC26A4*.

INTRODUCTION

Sensorineural hearing loss (SNHL) is the most common sensory disorder, affecting more than 1:1,000 newborns, with ~50% of cases attributed to genetic defects.¹ To date, ~199 causative genes associated with syndromic or non-syndromic SNHL have been identified.² Among them, recessive mutations in the *SLC26A4* gene cause Pendred syndrome (MIM: 274600) and non-syndromic hearing loss with enlarged vestibular aqueduct (EVA), also known as DFNB4

(MIM: 600791), two common deafness disorders that account for ~10% of all cases of hereditary hearing loss.^{3,4}

SLC26A4 consists of 21 exons and encodes a transmembrane protein of 780 amino acids, called pendrin, an electroneutral anion exchanger that transports negatively charged ions such as chloride, iodide, bicarbonate, formate, and thiocyanate across the cell membrane.⁵⁻⁷ Pendrin is highly expressed in the thyroid and inner ear. In the inner ear of mice, pendrin is expressed in a variety of non-sensory epithelial cells in a highly discrete pattern in the saccule, utricle, and ampulla, as well as in the endolymphatic sac.⁸ Mutations in *SLC26A4* impair or abolish the ion-transporting activity of pendrin, which disrupts proper development of the inner ear, leading to abnormal structures and failure to acquire normal hearing.^{9,10}

The *SLC26A4* c.919-2A>G mutation, hereafter referred to as A-2G, was almost exclusively detected in Asian populations.¹¹ It is the most prevalent pathogenic mutation in the gene in Chinese populations, responsible for ~60% of all *SLC26A4* disease mutant forms.¹² An earlier study has suggested that ~12.5% of Chinese children with SNHL carry this mutation.¹³ The A-2G mutation, which is located at the 3' splice site of intron 7, disrupts the highly conserved dinucleotide AG and causes predominant skipping of exon 8. The

Received 12 September 2021; accepted 18 March 2022;
<https://doi.org/10.1016/j.omtn.2022.03.015>.

⁹These authors contributed equally

Correspondence: Yimin Hua, Jiangsu Key Laboratory for Molecular and Medical Biotechnology, College of Life Sciences, Nanjing Normal University, Nanjing 210023, China.

E-mail: huay@njnu.edu.cn

Correspondence: Yilai Shu, ENT institute and Department of Otorhinolaryngology, Eye & ENT Hospital, State Key Laboratory of Medical Neurobiology, Fudan University, Shanghai 200031, China.

E-mail: yilai_shu@fudan.edu.cn



exon 8-skipped ($\Delta 8$) transcript is frameshifted in the last 13 exons and induces a premature termination codon (PTC) in exon 9, generating a truncated dysfunctional protein of only 310 amino acids.¹⁴

Currently, no effective drugs are available to treat SNHL, except for hearing aids and cochlear implants. Several strategies, such as stem cells, gene therapy, and antisense oligonucleotides (ASOs), have been attempted to treat hearing loss in mouse models of SNHL.¹⁵ Gene therapy holds promise to treat diseases caused by recessive mutations. Kim et al.¹⁶ showed that local embryonic delivery of normal *Slc26a4* cDNA using a recombinant adeno-associated virus (rAAV) vector restored the acquisition of hearing in pendrin-deficient mice. In contrast, ASO technology has been proved to be a powerful approach to treat diseases associated with aberrant RNA splicing.^{17,18} We have previously developed an ASO drug, called nusinersen, to treat spinal muscular atrophy (SMA) by correcting *SMN2* mis-splicing.^{19,20} A similar ASO approach has also been successfully applied to treat a mouse model of Usher syndrome, a syndromic SNHL.^{21–23}

Nearly all spliceosomal introns conform to the GT-AG rule. A systematic analysis of human RNA-seq reads predicted only 15 (0.0067%) to be GT-GG introns.²⁴ Although extremely rare, the presence of non-canonical splice sites in the human genome indicates that they are still recognizable in an ideal scenario. In this study, through multiple rounds of selection in a minigene system, we identified a lead ASO that markedly increased the full-length (FL) transcript in cultured peripheral blood mononuclear cells (PBMCs) derived from homozygous patients and in mouse tissues of humanized *Slc26a4* A-2G mice after treatment. Our data indicate that ASOs can improve splicing at non-canonical splice sites and are promising to treat SNHL caused by the A-2G mutation.

RESULTS

Exon 8 splicing of the *SLC26A4* A-2G mutant can be modulated

To characterize mis-splicing of *SLC26A4* exon 8 caused by the A-2G mutation, we constructed a *SLC26A4* minigene in the pCI-neo expression vector that comprises the genomic DNA fragment from exon 7 to the first 27 nt of intron 9 except for a shortened intron 8 (Figure 1A). The A-2G mutant was generated by site-directed mutagenesis. Plasmids were transiently transfected into four different cell types (HEK293, HeLa, U-87 MG, and HepG2), and the splicing patterns of the wild-type (WT) minigene and the A-2G mutant were examined using semi-quantitative fluorescent RT-polymerase chain reaction (PCR). As expected, the WT minigene expressed only the FL transcript (Figure 1B). Surprisingly, the mutant expressed two additional transcripts in all cell lines: one was due to exon 8 skipping and the other due to intron 7 retention (IR7) (Figure 1B). The unexpected IR7 transcript, which was more abundant than the other two transcripts, was not detected in prior studies with patient-derived cell samples.^{14,25} Although the splicing pattern of the mutant minigene appears not to faithfully mimic that of the endogenous mutant gene, the expression level of the FL isoform in HEK293 cells was much lower than that of the $\Delta 8$ isoform. Therefore, we deemed

that the minigene is still useful for analyzing splicing regulation and initial high-throughput drug screening.

Natural non-canonical splice sites are generally associated with distinctive features,²⁴ e.g., high enrichment of splicing regulatory elements (SREs) in the vicinity, giving an appropriate context for the weak splice sites to be efficiently processed. We wondered whether exon 8 splicing of the mutant minigene is still rescuable by testing the effects of a cohort of T7-tagged splicing factors, including serine and arginine-rich (SR) proteins and heterogeneous nuclear ribonucleoproteins (hnRNPs), on splicing of the mutant pre-mRNA. The mutant minigene and individual protein expression plasmids were co-transfected into HEK293 cells. Western blotting with an anti-T7 antibody showed that all proteins were properly expressed (Figure 1C). We calculated the percentages of both FL (% FL) and $\Delta 8$ (% $\Delta 8$) transcripts. Nine splicing factors enhanced expression of the $\Delta 8$ transcript, whereas three inhibited it (Figures 1D and 1E). Particularly, three SR proteins (SRSF2, SRSF8, and SRSF5) and HuR potentially repressed exon 8 splicing, as well as IR7, leading to predominant expression of the $\Delta 8$ isoform. Interestingly, the U1-specific protein SNRPA displayed the most stimulatory effect on exon 8 inclusion. These data highlight that exon 8 splicing of the mutant can be modulated, and design of ASOs to rescue exon 8 mis-splicing is a practical strategy.

Identification of ASOs that efficiently promote exon 8 inclusion of the mutant pre-mRNA

Intron and exon definition is often affected by not only the core splicing signals (the 5' and 3' splice sites, polypyrimidine tract, and branchpoint), but also nearby auxiliary signals, i.e., SREs. Ideally, ASOs should target strong exonic or intronic splicing silencers (ESSs or ISSs) to abrogate their inhibitory activities through steric occlusion by base-pairing. However, it is still challenging to precisely predict key splicing silencers. Therefore, we systematically screened a series of ASOs via two rounds of ASO walks and length optimization. We first designed fifteen 15-mer overlapping ASOs with uniform 2'-O-methoxyethyl ribose (MOE) ribose and phosphorothioate (PS) backbone, covering a 155-nt region from the third nucleotide of exon 8 to the 74th nucleotide of intron 8 (Figure 2A); each ASO was named based on the coordinates of its target sequence in exon 8 or intron 8. An unrelated oligonucleotide (ASO 0000) was used as a negative control. To test the effects of these ASOs, we co-transfected 100 nM of each ASO with the mutant minigene into HEK293 cells, and then exon 8 splicing was assayed by semi-quantitative fluorescent RT-PCR. As shown in Figures 2B and S1A, ASOs that target exon 8 or the 5' splice site of intron 8 caused predominant skipping of the exon; ASOs that target the region downstream of the 5' splice site generated complex results. One ASO (1024) that targets a sequence from position 10 to position 24 in intron 8 markedly increased the FL-transcript percentage from 20% (control) to 28%. ASO 1024 treatment also led to an increase in IR7. Due to the IR7 event, which is absent for the endogenous A-2G mutant in human cells, the actual effect of ASO 1024 on the FL transcript is most likely underappreciated in the minigene system. Therefore, we also used reduction in the percentage of exon 8 skipping as another criterion to evaluate ASO performance.

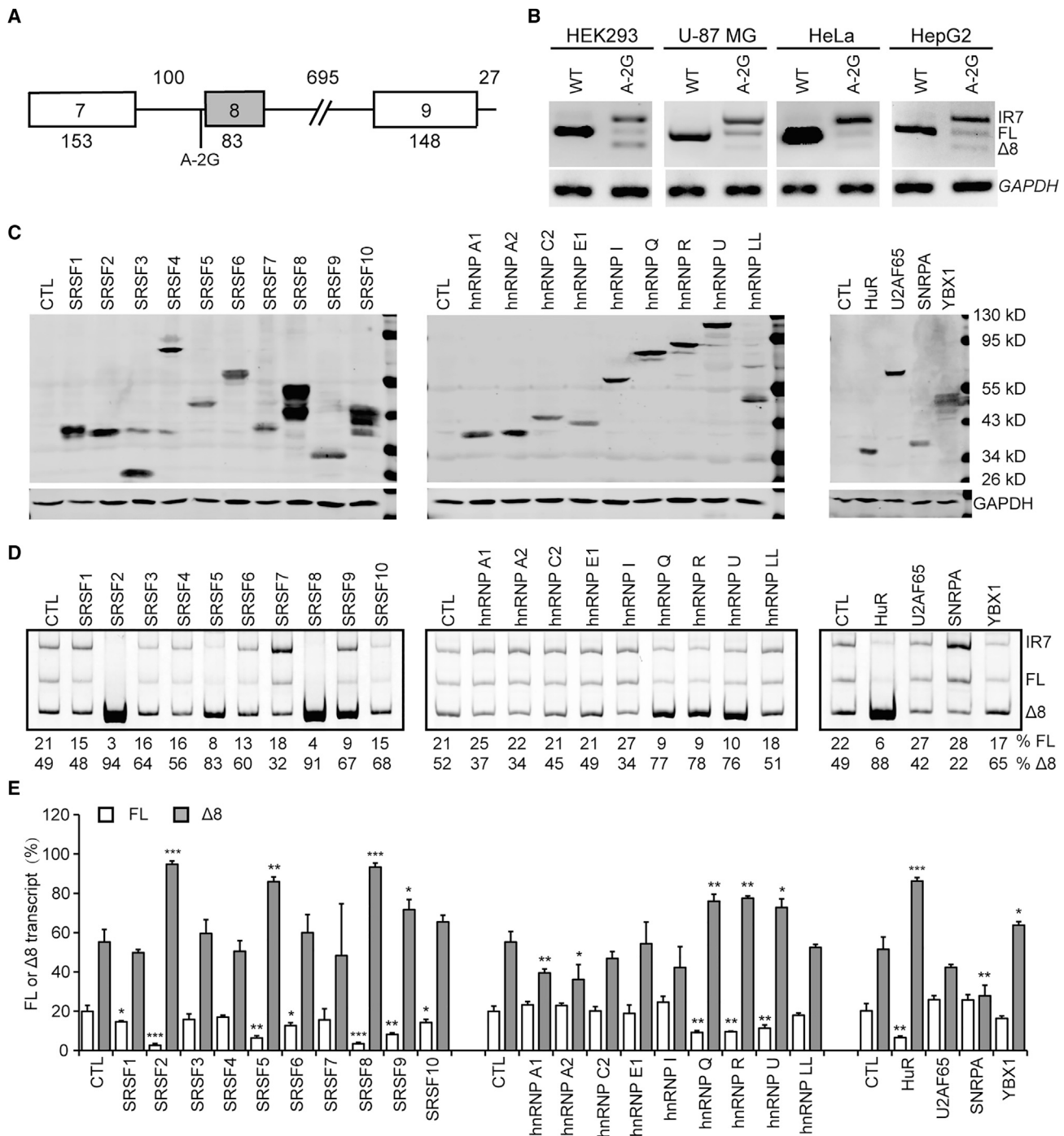


Figure 1. Splicing analysis of the SCL26A4 A-2G mutant minigene

(A) Diagram of the minigene. Exons are shown with boxes and introns with lines, and their lengths are indicated. (B) The splicing patterns of the WT and mutant minigenes were analyzed in four cell types: HEK293, U-87 MG, HeLa, and HepG2. RNA samples were analyzed by fluorescent RT-PCR. *GAPDH* was used as control. Three transcripts were detected in the mutant samples. (C) Western blot analysis of 23 splicing factors expressed in HEK293 cells using an anti-T7 antibody. *GAPDH* was used as a loading control. (D) Effects of overexpression of various splicing factors on the SCL26A4 A-2G minigene. A total of 500 ng of each expression plasmid was co-transfected with the mutant minigene (500 ng) into HEK293 cells, and RNA samples were analyzed as above. (E) Data from three independent experiments as shown in (D) were quantitated. * $p < 0.05$; ** $p < 0.01$; *** $p < 0.001$, all compared with CTL. Δ8, exon 8 skipped; A-2G, c.919-2A>G mutant; CTL, empty vector control; FL, full-length; IR7, intron 7 retention; WT, wild-type.

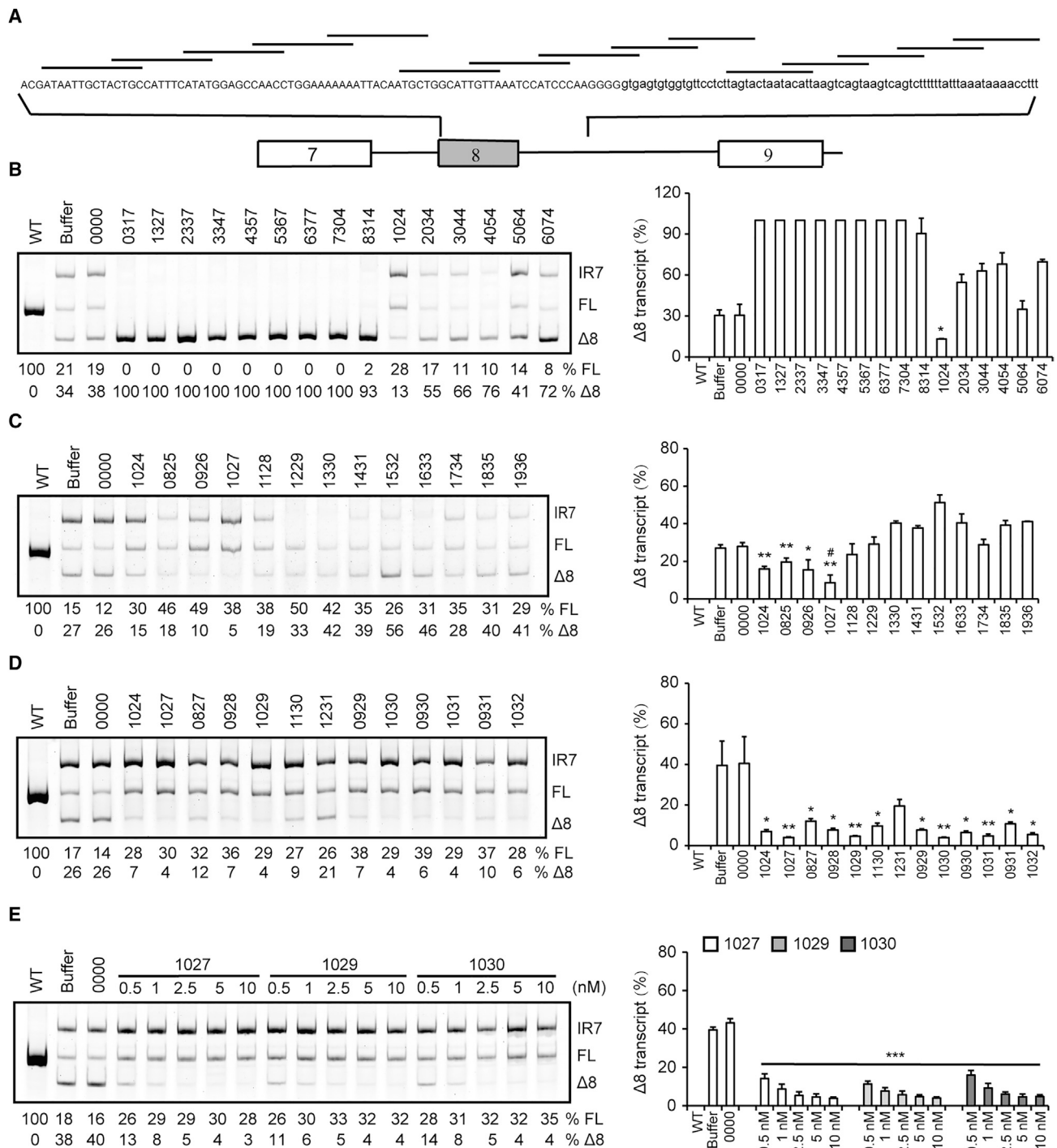


Figure 2. Systematic screening of ASOs that inhibit *SLC26A4* A-2G exon 8 skipping

(A) Schematic representation of ASOs used in the initial walk. ASOs cover a 155-nt region from the 3rd nucleotide of exon 8 to the 74th nucleotide of intron 8. (B) The effects of the initial walk ASOs were examined with the *SLC26A4* A-2G minigene in HEK293 cells. A total of 100 nM of each ASO was co-transfected with the mutant minigene (500 ng). Buffer only and an unrelated ASO 0000 were used as negative controls. (C) ASOs in the microwalk were analyzed. (D) ASO length optimization was performed. For both (C) and (D), 10 nM of each ASO was co-transfected with the mutant minigene into HEK293 cells. (E) The dose-response analysis of the top three ASOs. Five concentrations (0.5, 1, 2.5, 5, and 10 nM) were used. For (B–E), three independent experiments are quantitated on the right. **p* < 0.05, ***p* < 0.01, ****p* < 0.001, all compared with ASO 0000; #*p* < 0.05, compared with ASO 1024. WT, wild-type minigene without ASO treatment.

The goal of the initial ASO walk was to pinpoint a desirable target region in the pre-mRNA. To acquire more effective ASOs, we designed twelve 18-mer high-resolution microwalk ASOs focusing on the region identified above: ASOs positioned along the target with 1-nt steps. We co-transfected each ASO at 10 nM with the mutant minigene into HEK293 cells and examined exon 8 splicing. Compared with ASO 1024, ASOs 0825, 0926, 1128, and 1229 all markedly improved exon 8 splicing (Figure S1B), and ASO 1027 induced the lowest percentages of the $\Delta 8$ isoform (Figure 2C).

The length of ASOs impacts their effectiveness, but it is hardly predictable which length generates the maximal antisense activity. To obtain the optimal ASO, we tested 11 ASOs with varying lengths from 20 to 23 nt, all targeting the preferable region from position 8 to 32 in intron 8 based on the above ASO walks. Each ASO at 10 nM was co-transfected with the mutant minigene into HEK293 cells, and splicing changes were examined as described above. As shown in Figures 2D and S1C, most of the 11 ASOs showed similar effects on exon 8 splicing to that of ASO 1027. ASOs 1027, 1029, 1030, and 1031 all had the same lowest exon 8 skipping percentage. To distinguish the most effective ASO, we further conducted dose-response analysis of ASOs 1027, 1029, and 1030 at five concentrations: 0.5, 1, 2.5, 5, and 10 nM. All ASOs induced a pronounced increase of the FL transcript at 0.5 nM, and ASO 1029 treatment at the lowest concentration brought about the lowest exon 8 skipping percentage (Figures 2E and S1D).

The effect of ASO 1029 on patients' cells

To test whether the effect of ASO 1029 on splicing of the A-2G mutant minigene is conserved for the endogenous *SLC26A4* mutant, we harvested PBMCs from two patients with the A-2G homozygous mutation and cultured them in RPMI 1640 medium. PBMCs derived from a healthy subject were used as a positive control. Because PBMCs are refractory to ASO transfection, we attached a cholesterol molecule to the 3' end of ASO 1029 to facilitate spontaneous uptake of the ASO by suspended PBMCs.²⁶ Cholesterol-conjugated ASO 1029 at 2 μ M was added into low-serum complete medium with 10⁶ cells/well. Forty-eight hours post-treatment, PBMCs were collected for splicing analysis. As expected, the normal control PBMCs expressed only the FL transcript, whereas the patients' cells expressed the FL and $\Delta 8$ transcripts without IR7 observed (Figure 3A). We have validated the two transcripts by sequencing (Figure 3B). After ASO treatment, the percentage of exon 8 inclusion was markedly increased from 31% (untreated) to 67% and from 21.5% (untreated) to 61.5% for the two patients' cells, respectively. Notably, the PTC in exon 9 in the exon 8-skipped isoform is expected to trigger nonsense-mediated mRNA decay (NMD), and thus the actual exon 8 skipping extent in pre-mRNA splicing of the mutant should be more predominant than the observed values.

ASO 1029 promoted exon 8 splicing in a partially humanized mouse model

To assess the effect of ASO 1029 *in vivo*, we generated a chimeric *Slc26a4* mouse model by replacement of the 727-nt mouse genomic

fragment from the last 195 nt of intron 6 to the first 175 nt of intron 8 in the *Slc26a4* gene with the corresponding 794-nt human sequence (Figure 4A). We examined expression profiles of the WT chimeric (chi-WT) and mutant chimeric (chi-Mut) *Slc26a4* genes (see Materials and methods) in several tissues of neonatal mice that were homozygous for either allele, and we detected high mRNA levels of both genes in the kidneys, inner ears, and lungs, and low levels in the heart, brain, and liver. The tissue expression profiles of the chi-WT and chi-Mut alleles were comparable overall with that of the WT mouse allele (Figure 4B). Unexpectedly, aside from the FL and $\Delta 8$ isoforms, we also detected the IR7 isoform in the chi-Mut mouse tissues as in the minigene, and it was particularly prominent in the inner ear and kidney tissues. More surprisingly, we observed the IR7 transcript in some chi-WT mouse tissues, such as the brain and heart, despite the band being faint (Figure 4B). Because the humanized sequence part in the chi-WT setting harbors all the core splicing signals of intron 7, the observed intron retention event in this case is perplexing, which will require further investigation to understand the underlying mechanism.

Although the chi-Mut mouse model is not ideal, we were still curious if ASO 1029 could somehow rescue mis-splicing of the chi-Mut gene. Pendrin is essential for early inner ear development. Therefore, we tested the effect of ASO 1029 in neonatal mice. Two subcutaneous ASO injections at 160 mg/kg were administered to homozygous chi-Mut pups on post-natal day (P) 3 and P4. Liver, kidney, and inner ear tissues were collected on P7. In the liver, we observed a pronounced increase in the FL-transcript percentage from 13% in the saline control group to 28% in ASO-treated mice. But no significant exon 8 splicing changes in inner ear and kidney samples were observed (Figure 4C). We also quantitated tissue FL-transcript levels using qRT-PCR; ASO treatment increased the FL transcript by 2.5-fold in the liver and 1.6-fold in the kidneys, but no changes were observed in the inner ears (Figure 4D). Moreover, we performed western blot analysis of mouse liver extracts and observed a 2.2-fold increase in pendrin levels in mice treated with ASO 1029 (Figure 4E).

Mechanism of action of ASO 1029

The potent stimulatory effect of ASO 1029 supports the presence of a strong ISS in the target region; we termed it ISS-F1. Indeed, positions 20–22 are UAG, a known binding motif of hnRNP A/B family proteins,²⁷ and hnRNP A1 and its paralog protein hnRNP A2 are well-known splicing repressors. To verify that UAG is indeed responsible for the silencing activity of ISS-F1, we generated five deletion mutations (D10-13, D14-17, D18-21, D22-25, and D26-29) at positions 10–29 in intron 8 in the setting of the A-2G mutant minigene (Figure 5A); splicing changes of these double mutants were evaluated in HEK293 cells. Compared with the parental A-2G mutant minigene, two mutants, D18-21 and D22-25, both with the UAG motif being disrupted, displayed a marked increase in expression of the FL transcript, whereas the other three mutants displayed a moderate decrease (D10-13 and D14-17) or no changes (D26-29). Similar to what we observed earlier in ASO screening (Figure 2), an increase in the FL-transcript percentage for mutants D18-21 and D22-25 accompanied an increase in IR7, leading to drastic reduction in exon 8 skipping.

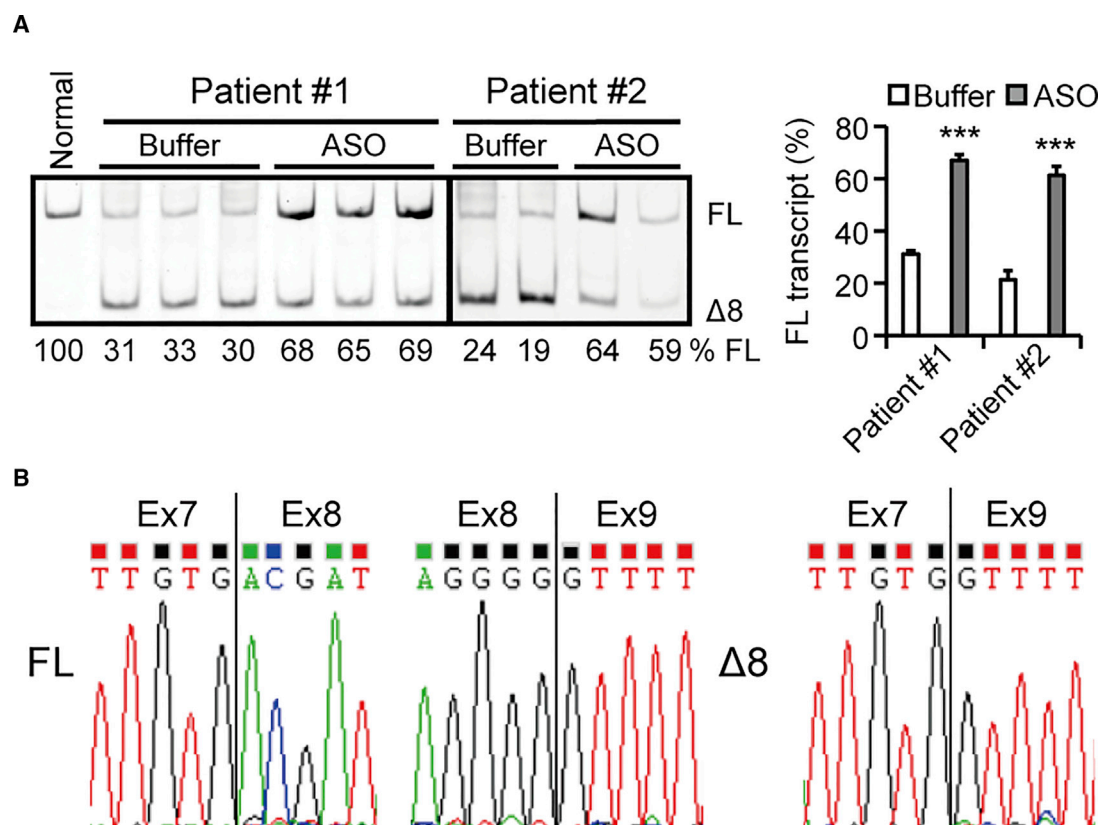


Figure 3. ASO 1029 promoted exon 8 inclusion of the *SLC26A4* A-2G mutant in PBMCs derived from two homozygous patients

(A) The effect of cholesterol-conjugated ASO 1029 at 2 μ M on the endogenous *SLC26A4* A-2G mutant of the cultured homozygous PBMCs was examined. Cells were collected 48 h after ASO treatment. PBMCs derived from a healthy subject (normal) were used as a positive control, and buffer only was used as a negative control. RNA splicing was analyzed by Cy5-labeled RT-PCR. Quantitation of the data ($n = 3$ or 2) is shown on the right. (B) Sequencing data of the two transcripts shown in (A). *** $p < 0.001$. % FL, percentage of the FL transcript.

Our data indicate that the core sequence of ISS-F1 is within the 8-nt deletion region (CTTAGTAC). To narrow down the core sequence, we generated four more deletion mutants D18-19, D20-22, D21-22, and D23-25. As shown in Figure 5B, only D20-22 and D21-22, in which UAG or AG was deleted, resulted in a dramatic decrease of the $\Delta 8$ transcript. The data clearly demonstrated that the UAG motif at positions 20–22 is responsible for the inhibitory activity of ISS-F1. We also generated five replacement mutations (Rep1–5) at the UAG site that either abolishes, weakens, or improves the binding affinity of the site for hnRNP A1/A2. We used an hnRNP A1 position weight matrix (PWM) with background correction (A1_winBG), which was previously derived from SELEX (systematic evolution of ligands by exponential enrichment) data.²⁸ The percentage of exon 8 skipping of each mutant was plotted against its calculated hnRNP A1 score.²⁹ We observed a strong correlation between the extent of exon 8 skipping of these double mutants and the corresponding motif scores: the coefficient of determination (R^2) is 0.9833 (Figures 5C–5E).

The above mutagenesis analysis indicates that the silencing activity of ISS-F1 is mediated by hnRNP A1/A2. However, both hnRNP A1

and A2 did not significantly alter the FL isoform levels but rather promoted IR7 through reducing the $\Delta 8$ isoform levels (Figures 1D and 1E). We also examined the effect of co-knockdown of hnRNP A1 and A2 on splicing of the A-2G mutant minigene using previously described small interfering RNAs (siRNAs).²⁹ After siRNA treatment, mRNA levels of either *hnRNP A1* or *A2* were decreased to about 50%, and a robust increase of the $\Delta 8$ isoform, as well as a decrease of both the IR7 and FL isoforms, was observed (Figure 6A). These data suggest that hnRNP A1 and A2 affect pre-mRNA splicing of the mutant via multiple mechanisms by binding to different regions. Indeed, numerous hnRNP A1-binding motifs, including UAG and its weak version CAG, are present in various regions of the minigene. For example, three UAG repeats are located immediately downstream of the 5' splice site of intron 7, which likely contributes to IR7. Therefore, we tested the effects of co-knockdown and overexpression of hnRNP A1 and A2, respectively, on the Rep2 mutant, in which UAG in ISS-F1 has been abolished. As shown in Figures 6B and 6C, hnRNP A1/A2 still displayed stimulatory activity on IR7 at the expense of the other two isoforms for the double-mutant minigene.

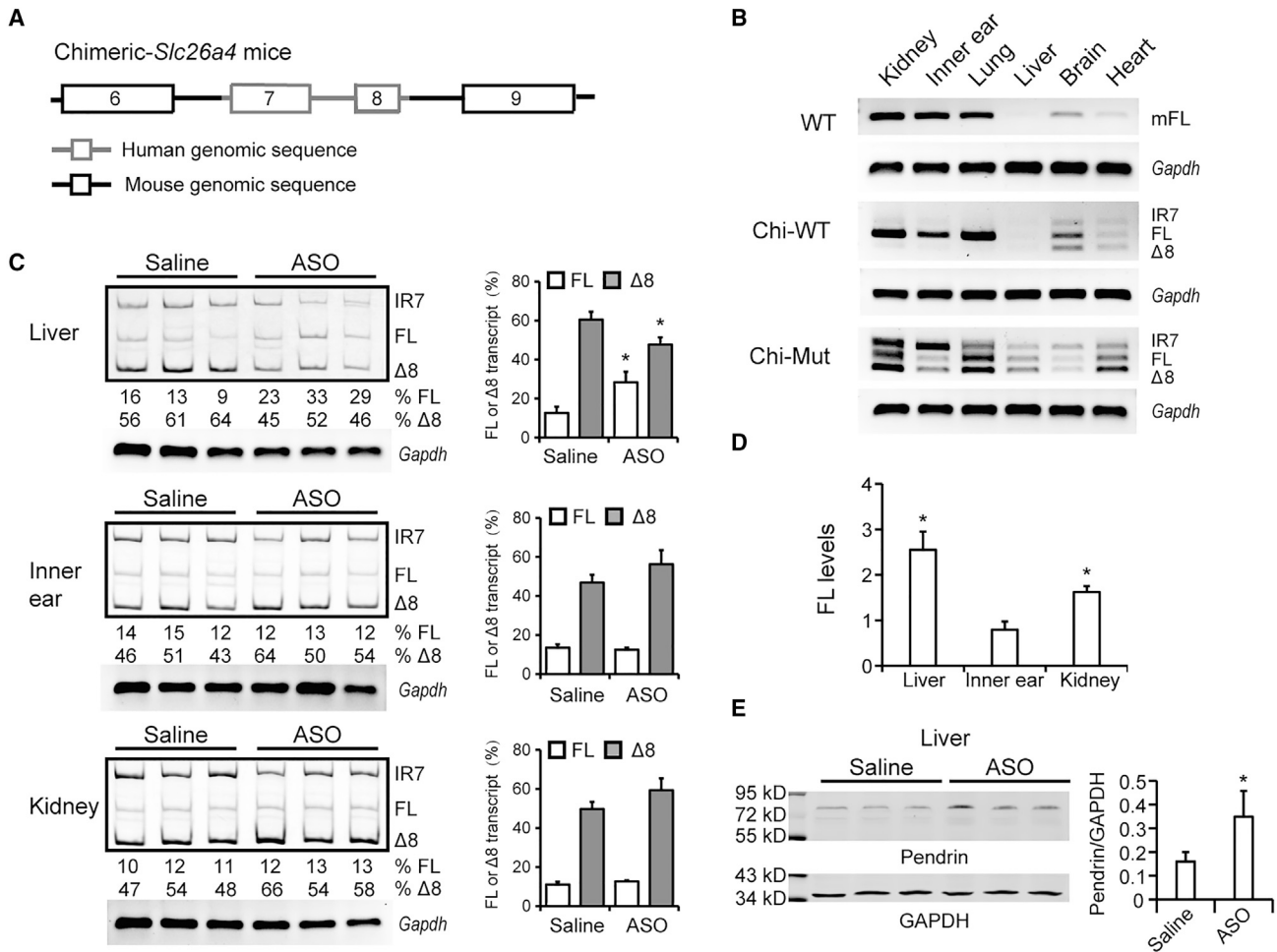


Figure 4. The effect of ASO 1029 on splicing of the chimeric *Slc26a4* A-2G gene in a partially humanized mouse model

(A) Diagram of the chimeric gene. Human genomic part is shown in gray. (B) Analysis of mRNA expression of the *Slc26a4* or chimeric genes in six tissues of homozygous WT, chi-WT, and chi-Mut mice on P7, respectively. *Gapdh* was used as control. (C) Splicing analysis of the chi-Mut gene in the liver, inner ears, and kidneys of homozygous mice on P7 after two subcutaneous injections of ASO 1029 at 160 mg/kg per injection between P3 and P4. Quantitation of the data ($n = 3$) is shown on the right. (D) FL-transcript levels of ASO-treated mice ($n = 3$) were analyzed by qRT-PCR. Data were normalized to *Gapdh* and presented as fold changes compared with saline-treated mice. (E) Western blot analysis of pendrin in the liver of the homozygous chi-Mut mice after saline or ASO treatment. GAPDH was used as loading control. (C–E) * $p < 0.05$, all compared with saline control.

To determine whether hnRNP A1 suppresses exon 8 splicing when bound to ISS-F1, we took advantage of an MS2 tethering splicing assay (Figure 6D), in which a protein of interest is fused to bacteriophage MS2 coat protein (CP) and co-expressed in cultured cells with a pre-mRNA substrate that harbors a copy of the MS2 hairpin sequence at a position of interest, so that the effect of the protein of interest on splicing of the substrate at a specific site can be analyzed.³⁰ Two plasmids were generated: one expresses CP-fused hnRNP A1 (T7-CP-A1), and the other expresses a double-mutant minigene (named A-2G/MS2) with UAG in ISS-F1 being replaced with the MS2 hairpin sequence. Plasmids were co-transfected into HEK293 cells, and exon 8 splicing of the A-2G/MS2 minigene was analyzed (Figures 6E and 6F). T7-CP-A1 slightly increased the FL isoform of the parental A-2G minigene but decreased the isoform of the A-2G/

MS2 minigene, supporting our notion that ISS-F1 is an hnRNP A1/A2-mediated silencer.

To further prove that hnRNP A1 binds specifically to ISS-F1, we performed RNA-affinity chromatography. Two 16-nt biotinylated RNA species with sequences corresponding to nucleotide positions 10–25 in intron 8 of the WT *SLC26A4* gene and Rep2 mutant, respectively, were obtained commercially and immobilized onto streptavidin beads. Each RNA was incubated with HEK293 nuclear extract (NE), and proteins that remained bound to the RNA after extensive washing with buffer containing 100 mM KCl were analyzed with SDS-PAGE and then Coomassie blue staining. A prominent ~34-kDa band in the WT-RNA protein samples was revealed by Coomassie blue staining, but not in the mutant-RNA samples (Figure 6G).

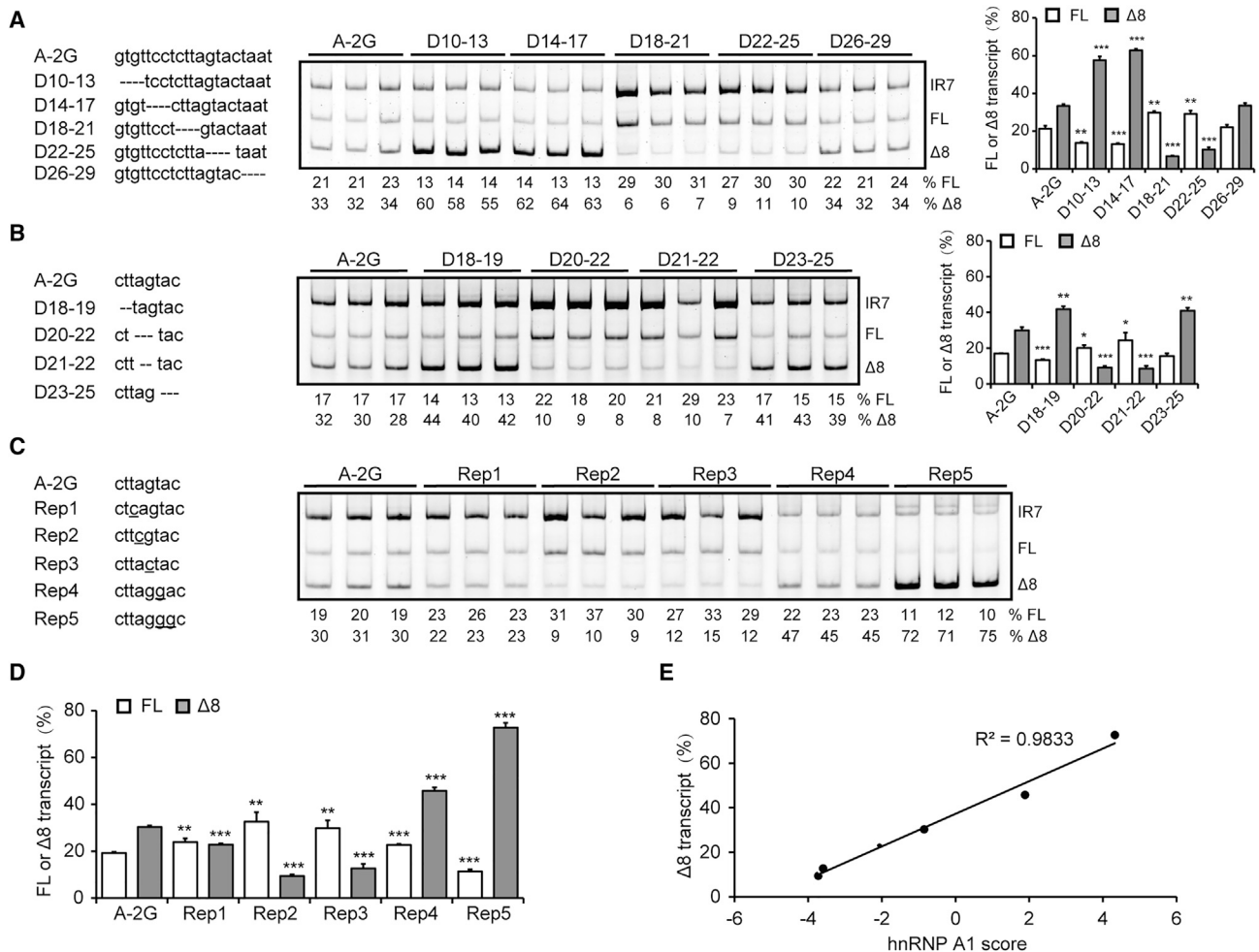


Figure 5. Mutational analysis of the target region of ASO 1029 in intron 8 of the *SLC26A4* A-2G minigene

(A) The first round of deletion analysis. All deletions are indicated by dashed lines. A total of 500 ng of each mutant plasmid was transfected into HEK293 cells, and splicing was analyzed 30 h post-transfection. Quantitation of the data ($n = 3$) is shown on the right. (B) The second round of deletion analysis. (C) Analysis of five replacement mutations (underlined). (D) Quantitation of the data ($n = 3$) shown in (C). (E) Percentages of the $\Delta 8$ transcript were plotted against calculated hnRNP A1 scores as a scatterplot; $R^2 = 0.9833$. (A, B, and D) * $p < 0.05$, ** $p < 0.01$, *** $p < 0.001$, all compared with the parental A-2G mutant.

Western blotting with an anti-hnRNP A1 antibody confirmed that the 34-kDa band indeed is hnRNP A1 (Figure 6H).

DISCUSSION

Mis-splicing of the *SLC26A4* pre-mRNA induced by the recessive intronic mutation A-2G is a leading genetic cause of SNHL in East Asia. The splice-site mutation breaks the “GT-AG” splicing rule in intron 7 and causes predominant skipping of the downstream exon accompanied by a frameshift. Apparently, correction of *SLC26A4* mis-splicing to increase its normal protein product is a promising strategy to treat the subset of patients. In this study, we first built a *SLC26A4* mutant minigene and examined the effects of multiple splicing factors on pre-mRNA splicing of the minigene, which verified that mis-splicing induced by the non-canonical 3' splice site remains rescuable. We then performed a systematic

screening of ASOs designed to target negative splicing *cis* elements within and near exon 8 using the mutant minigene in HEK293 cells. Through three rounds of selection with ASO walks and length optimization from 38 ASOs, we identified a few that potently promote exon 8 splicing of the mutant pre-mRNA at low concentrations. One lead ASO 1029 markedly improved exon 8 inclusion during pre-mRNA splicing of the endogenous A-2G mutant in cultured PBMCs derived from SNHL patients. Moreover, administration of ASO 1029 at 160 mg/kg/day for 2 consecutive days increased the FL transcript in the liver of a humanized mouse model, suggesting that ASO 1029 has therapeutic potential. Finally, using mutagenesis, RNA-affinity chromatography, western blotting, and an MS2-tethering assay, we revealed the mechanism of action of ASO 1029, which operates via occlusion of an hnRNP A1/A2-mediated ISS in intron 8.

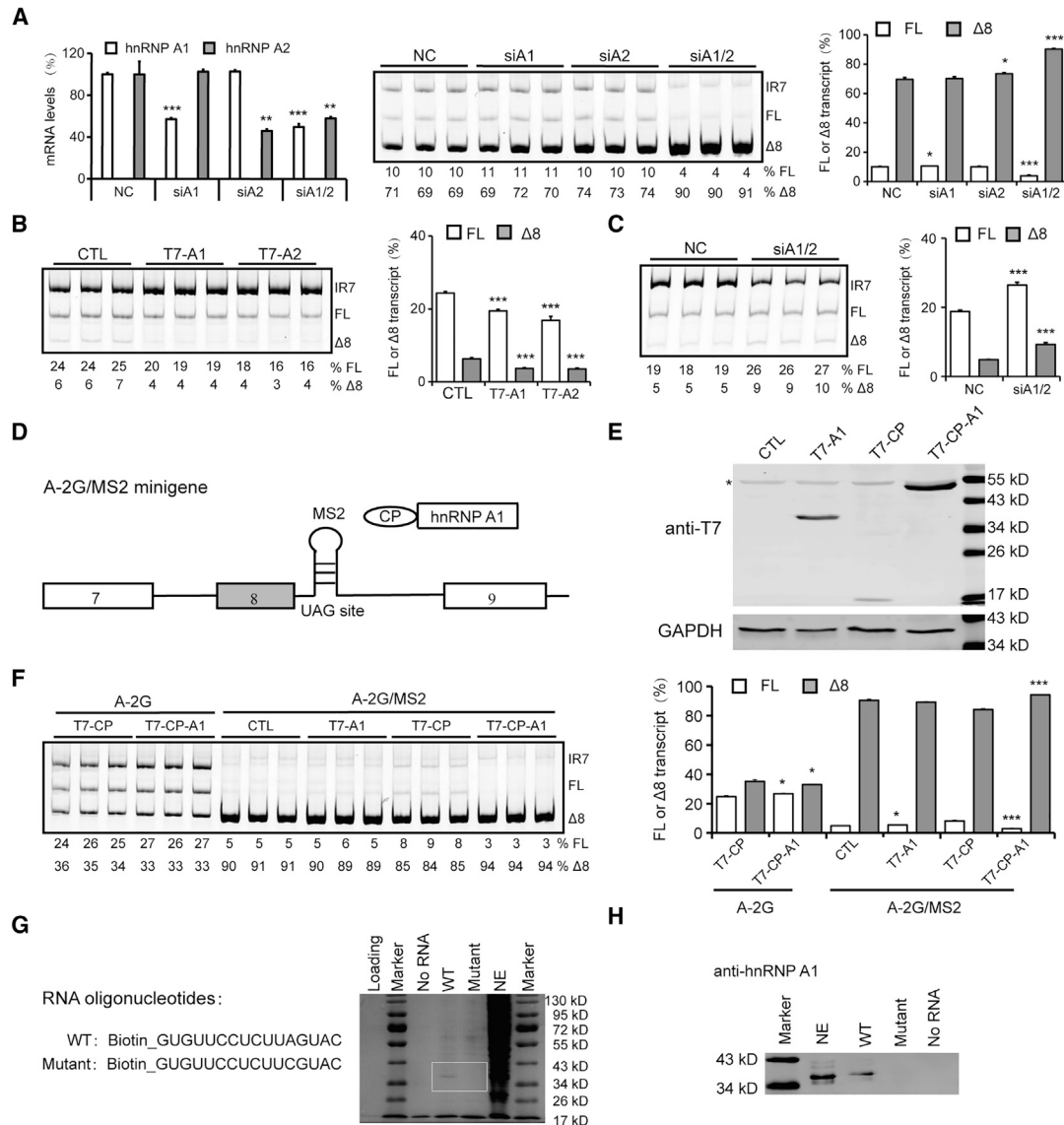


Figure 6. hnRNP A1/A2 bind to the ISS-F1 and repress *SLC26A4* exon 8 splicing

(A) The effect of siRNA knockdown of *hnRNP A1* (siA1), *hnRNP A2* (siA2), or co-knockdown (siA1/2). A total of 50 nM of each siRNA was co-transfected with 500 ng of the *SLC26A4* A-2G minigene into HEK293 cells. An unrelated siRNA was used as negative control (NC). mRNA levels were analyzed by qRT-PCR. Data were normalized to *GAPDH* and presented as fold changes compared with NC (n = 3). (B and C) The effects of overexpression (B) or co-knockdown (C) of *hnRNP A1* and *A2* on splicing of mutant Rep2 in HEK293 cells; quantitation of the data (n = 3) is shown on the right. (D) Diagram of the *SLC26A4* A-2G/MS2 minigene. The trinucleotide UAG in ISS-F1 was replaced by the MS2 hairpin sequence so that MS2 coat protein-fused *hnRNP A1* (CP-A1) can specifically bind to this position. (E) Western blot analysis of T7-A1, T7-tagged coat protein (T7-CP), and T7-tagged CP-A1 (T7-CP-A1) expressed in HEK293 cells using an anti-T7 antibody. *GAPDH* was used as loading control. Asterisk (*) indicates non-specific band. (F) The effect of T7-CP-A1 on the A-2G/MS2 minigene (n = 3). A total of 500 ng of each plasmid was co-transfected with 500 ng of the parental A-2G or A-2G/MS2 minigene in HEK293 cells. T7-A1 and T7-CP were used as controls. (G) The 16-nt biotinylated RNA and its mutant Rep2 were used for RNA-affinity chromatography. Biotinylated RNAs, immobilized onto streptavidin beads, were incubated with HEK293 cell nuclear extract (NE). After washing with buffer, captured proteins were eluted and analyzed with SDS-PAGE, followed by Coomassie blue staining. A protein band around 34 kDa was prominent on the gel in the WT RNA sample, but not in the mutant sample. (H) Western blot analysis of eluted proteins with an anti-*hnRNP A1* antibody confirmed the 34-kDa band indeed is *hnRNP A1*. For all histograms, *p < 0.05, **p < 0.01, ***p < 0.001, all compared with negative controls (NC, CTL, or T7-CP). NE, 20 μ L NE loaded; no RNA, no RNA used; T7-A1, T7-tagged *hnRNP A1*; T7-A2, T7-tagged *hnRNP A2*.

Pendrin functions as an anion exchanger in multiple tissues, including the inner ears, thyroid, kidneys, and airways. It is particularly essential for development of the inner ear. Using an inducible mouse model, Choi et al.⁸ revealed that *Slc26a4* expression from embryonic day (E) 16.5 to P2 is crucial for acquisition of normal hearing. Li et al.³¹ further identified the endolymphatic sac as the critical location for *Slc26a4* expression, and expression therein alone was sufficient for both structural and functional inner ear development. These findings defined both temporal window and spatial requirement for therapeutic intervention in the context of loss-of-function *SLC26A4* mutations. However, many *SLC26A4* mutations remain partially functional, reflected by the considerable clinical variability in inner ear and thyroid phenotypes and the progressive and fluctuating nature of hearing loss.^{25,32} With respect to the A-2G mutation, we showed that a small percentage of the FL transcript was still expressed in PBMCs derived from homozygous patients (Figure 3), consistent with an earlier study in which both the FL and $\Delta 8$ transcripts were detected, although with varying ratios, in nasal mucosa and lymphocyte samples derived from two patients.²⁵ This explains that patients with the A-2G mutation in both alleles present better phenotype, including better residual hearing compared with some other mutations.²⁵ Collectively, the mutant expression pattern and clinical manifestations of the subset of SNHL highlight that treatment with an effective splice-switching molecule is feasible, and an earlier treatment should result in a better therapeutic outcome.

Several MOE- or morpholino-modified ASOs have been approved to treat two neuromuscular disorders, i.e., SMA and Duchenne muscular dystrophy (DMD), through redirecting pre-mRNA splicing of disease-associated genes. Nusinersen was initially identified from a large-scale ASO screen with an *SMN2* minigene.³³ Here we used a similar strategy to screen ASOs in a minigene context. The minigene system was chosen also because *SLC26A4* is expressed in limited cell lines probably because of hypermethylation of the gene,³⁴ and no cell lines carrying the A-2G mutation in the endogenous gene are available. Although the minigene differs from the mutated endogenous gene by expressing an extra intron retention isoform, using two parameters, i.e., increase in the FL transcript percentage and reduction in the $\Delta 8$ transcript percentage, we found several ASOs with therapeutic potential. We selected ASO 1029 as the winner mostly based on its capability in inhibiting exon 8 skipping at low concentrations in cultured cells. Although we cannot rule out the possibility that other top ASOs may be superior to ASO 1029 *in vivo*, its robust splicing-correcting effect on the endogenous mutant gene in patients' PBMCs that bear the correct genotype supports further study of the ASO (1029) as a drug candidate in animal models. Our data also indicate that mis-splicing caused by canonical splice-site disruptions can still be rescued. This opens the door to other approaches, e.g., small molecules, to fix mis-splicing of the mutant.

Unfortunately, the partially humanized *Slc26a4* A-2G allele in the mouse model generated in the present study, resembling the minigene, does not accurately mimic the human endogenous A-2G mutant. New transgenic mice harboring, e.g., the complete sequence

of the human A-2G mutant allele, should be generated to test the effect of ASOs without interference from the IR7 transcript. Nonetheless, we still observed a 2.5-fold increase of the FL transcript in the liver and 1.6-fold in the kidneys of the flawed mouse model, although not in the inner ears, following subcutaneous administration. The data are consistent with the absorption, distribution, metabolism, and excretion (ADME) properties of ASOs,³⁵ because liver cells are the main cell type that spontaneously takes up ASOs. We have also tried direct injection into cochlea of the inner ear (data not shown), but because of the small lymph volume, only a small quantity of ASO could be injected. Indeed, we did not observe better ASO accumulation in the inner ear tissues using this method compared with subcutaneous delivery (Figures S2 and S3). In the future, several strategies can be adopted to improve ASO effectiveness. First, we did not observe any signs of ASO toxicity after treatment; the dosage per administration and dosing frequency can be increased. Second, other delivery routes, such as intratympanic injection, can be tried to increase the initial ASO accumulation in the inner ears. Moreover, multiple chemical-conjugate approaches, as well as carrier-based delivery systems, are available or under development to enhance the ADME properties of ASOs.³⁵ In the future, with assistance of these novel techniques, sufficient ASO tissue penetration and cellular internalization in the inner ear may be achieved.

One puzzling observation in our study is that the mutant minigene, the chi-Mut allele, and, to a less extent, the chi-WT allele in mouse tissues produce an extra transcript, in contrast with the natural mutant allele in patient cells that expresses only the FL and $\Delta 8$ transcripts. It is possible that the patient endogenous allele expresses a small amount of the IR7 isoform during pre-mRNA splicing but is being degraded by the NMD pathway. For the minigene, because exon 9 is the last one, neither the $\Delta 8$ nor IR7 isoform should trigger strong NMD, providing a possible explanation for the presence of these three transcripts. However, the NMD mechanism cannot explain prominent expression of the IR7 isoform by the chi-Mut gene in the mouse model. And more puzzling is that the chi-WT gene, in which no splicing signals are disrupted, also expresses the three isoforms in some tissues, suggesting the involvement of other unknown mechanisms in promoting IR7.

Currently, we do not understand why multiple SR proteins promoted exon 8 skipping of the mutant minigene, which will require further study. SNRPA, a component of U1 small nuclear ribonucleoprotein particle (snRNP), repressed exon 8 skipping, suggesting that improvement of 5' splice-site recognition stimulates splicing of the exon. One striking observation is that all ASOs that target exon 8 caused complete skipping of the exon (Figure 2B), highlighting the presence of multiple splicing enhancers in exon 8. This may partly explain why 19%–33% of the FL transcript was still expressed in the patients' PBMCs (Figure 3). Therefore, the A-2G mutation case appears to resemble those rare natural non-canonical splice sites, which are surrounded by high density of SREs that help their recognition.²⁴ We noted that none of those previously developed therapeutic splice-switching ASOs target mis-splicing caused by disruption of canonical

splice sites. Our data prove that these mis-splicing events are still rescuable. Splicing mutations account for ~9% of all mutations logged in the Human Gene Mutation Database (HGMD; accessed on January 22, 2022),³⁶ among which about 73% occur at the conserved dinucleotides,³⁷ and a total of 2,474 entries are –2A>G mutations. We believe that ASOs hold promise for treating many diseases caused by splice-site mutations.

All the effective ASOs that we identified target ISS-F1, which is located immediately downstream of the 5' splice site of intron 8. Mutational analysis demonstrated that UAG in ISS-F1 is responsible for the silencing activity of the silencer. Although we did not observe significant increase of the FL transcript when hnRNP A1/A2 were depleted or decrease when hnRNP A1/A2 were over-expressed, because of the presence of multiple hnRNP A1/A2 motifs in other regions, the MS2-tethering method clearly showed that ISS-F1 is mediated by hnRNP A1/A2. Interestingly, the location of the target sequence and mechanism of action of ASO 1029 in the present study are almost identical to those of nusinersen, the ASO drug for treatment of SMA.³³ Potent ASOs were also reported to rescue exon splicing by targeting similar locations in *IKBKAP* and *ACADM*,^{38–40} hinting that the region immediately downstream of the 5' splice site of an alternatively spliced exon is often a favorite target for splicing-correcting ASOs, possibly because of both the frequent occurrence of ISSs and easy accessibility of ASOs to the region.

MATERIALS AND METHODS

Plasmids

The *SLC26A4* minigene comprising the 153-nt exon 7, the 100-nt intron 7, the 83-nt exon 8, a 695-nt shortened intron 8, the 148-nt exon 9, and the first 27 nt of intron 9 was constructed into the pCIneo vector by restriction enzymes XhoI, XbaI, and NotI (New England Biolabs, Ipswich, MA, USA). Genomic DNA fragments were amplified from HEK293 cells. Minigene mutants were generated by site-directed mutagenesis using partially overlapping primer sets. Protein-expression plasmids for all splicing factors, the bacteriophage MS2 CP, and the CP-fused hnRNP A1 were created by the SLIC (sequencing- and ligation-independent cloning) method using the pCGT7 vector;⁴¹ all expressed proteins had an N-terminal T7 tag and thus could be detected by an anti-T7 antibody.

Cell culture and transfections

The study of patients' PBMCs received ethical approval from the Institutional Review Board of the Eye and ENT Hospital of Fudan University. All subjects signed an informed consent. PBMCs were isolated from blood samples of two homozygous patients carrying the A-2G mutation and a healthy control subject by density gradient centrifugation and cultured in RPMI 1640 medium (Life Technologies). HEK293, HeLa, U-87 MG, and HepG2 cells were cultured in Dulbecco's modified Eagle's medium (Life Technologies, Carlsbad, CA, USA). Media were supplemented with 10% (v/v) fetal bovine serum (FBS), 100 U/mL penicillin, and 100 µg/mL streptomycin; cells were cultured at 37°C in a humidified 5% CO₂ atmosphere. For splicing analysis, 500 ng of each WT or mutant minigene plasmid

was transfected into 4×10^5 cells with or without a protein-expression plasmid using branched polyethylenimine (Sigma-Aldrich, St. Louis, MO, USA) in 12-well plates. All ASOs, including cholesterol-conjugated ASO 1029, were uniformly modified with MOE, PS backbone, and all 5-methyl cytosines. ASOs and siRNAs were purchased from Biosyntech (Suzhou, Jiangsu, China); all sequences are listed in Table S1. For ASO screening and gene knockdown, each ASO/siRNA or both siRNAs (for co-knockdown) were co-transfected with corresponding WT or mutant minigene plasmid into HEK293 cells using Lipofectamine 2000 (Life Technologies). For ASO analysis in PBMCs, 10^6 cells/well in a six-well plate were cultured in RPMI 1640 medium with 3% FBS, and cholesterol-conjugated ASO 1029 was added in the medium for 48 h.

Animals and oligonucleotide treatment

Mouse protocols used in the study were approved by the Institutional Animal Care and Use Committee of Fudan University (China). The SNHL mouse model was generated by Bioray Laboratories (Shanghai, China) in the C57BL/6 background, in which the 727-nt genomic DNA fragment of the mouse *Slc26a4* gene, including the last 195 nt of intron 6, the 153-nt exon 7, the 121-nt intron 7, the 83-nt exon 8, and the first 175 nt of intron 8, was replaced by the corresponding 794-nt sequence of the human *SLC26A4* gene, including the last 189 nt of intron 6, the 153-nt exon 7, the 100-nt intron 7, the 83-nt exon 8, and the first 269 nt of intron 8. The chimeric *Slc26a4* allele with the WT human sequence or the A-2G mutant was named as chi-WT or chi-Mut, respectively. The mouse model was maintained from breeding pairs (*Slc26a4*^{+/chi-Mut} × *Slc26a4*^{chi-Mut/chi-Mut}) in the Department of Laboratory Animal Science, Fudan University. Neonatal mice (*Slc26a4*^{chi-Mut/chi-Mut}) were subcutaneously injected twice with non-conjugated ASO 1029 at 160 mg/kg or equal volume of saline (control) with one injection on P3 and the other on P4; tissues were sampled on P7.

RT-PCR

Total RNA was isolated from cultured cell lines or mouse tissues using TRIzol reagent (Vazyme, Nanjing, Jiangsu, China) and from PBMCs using DNA/RNA/Protein Isolation Kit (OMEGA Bio-tek, Norcross, GA, USA). Then, 1 µg of each total RNA sample was reverse transcribed to cDNA with M-MLV (H⁻) reverse transcriptase (Vazyme) in a 20-µL reaction. To analyze splicing of the WT and mutant *SLC26A4* minigenes, we amplified transcripts with 32 cycles (95°C for 15 s, 58°C for 15 s, and 72°C for 30 s) by semi-quantitative fluorescent PCR with Cy5-labeled forward primer SLCE7-F (5'-Cy5-ACGCTGGTTGAGATTTTTCA-3') and reverse primer SLCT3-R (5'-TAACCCTCACTAAAGGGAAGC-3'). To analyze RNA splicing of the endogenous *SLC26A4* mutant in PBMCs, we amplified transcripts by 35 cycles with the Cy5-labeled SLCE7-F and reverse primer SLCE9-R (5'-GTTCCCATCGATGGTGT AATC-3'). To analyze RNA splicing of the chimeric *Slc26a4* gene with the A-2G mutation in mouse tissues after ASO treatment, we amplified transcripts by 35 cycles with the Cy5-labeled SLCE7-F and reverse primer mSlcE9-R (5'-CTGGTTCCTCCCATCGATGACATAG-3'). Cy5-labeled PCR products were separated on 6% native polyacrylamide

gels, and fluorescence images were acquired using FluorChem M (Alpha Technologies, Bellingham, WA, USA).

Standard RT-PCR was performed to detect expression of the mouse WT and chimeric *Slc26a4* genes in different tissues using two primer sets, respectively: mSlcE7-F (5'-ACACCAATATTGCCGATTTTCAT C-3') and mSlcE9-R, as well as SLCE7-F (5'-ACGCTGGTTGAGATTTTTC A-3') and mSlcE9-R. *Gapdh* was used as a reference gene with primers Gapdh-F (5'-CCGTAGACAAAATGGTGAAGGT-3') and Gapdh-R (5'-CGTGAGTGGAGTCATACTGGAA-3'). Quantitative real-time RT-PCR was performed on the StepOnePlus System (Thermo Fisher Scientific, Waltham, MA, USA) using FastStart Universal SYBR Green Master (Roche Applied Science, Indianapolis, IN, USA). The primer sets for detecting *hnRNP A1* and *hnRNP A2* mRNA levels are A1-F (5'-ACAACCTTCGGTCGTGG AGGAAACT-3'), A1-R (5'-CCAAAATTGCTTCCATCATTACCA A-3'), A2-F (5'-GCTGTAGCAAGAGAGGAATCTGGA-3'), and A2-R (5'-GCTTCTTACAGTTACATGAGCCC-3'); *GAPDH* was used as a reference gene with primers GAPDH-F (5'-AAGGTGAAG GTCGGAGTCAACGG-3') and GAPDH-R (5'-CCACTTGATTTT GGAGGGATCTC-3'). The primer sets for detecting the FL chi-Mut *Slc26a4* transcript in mouse tissues after ASO treatment are SlcE7-F (5'-CCTATAGAAGTAATTGTGACGA-3') and SlcE9-R (5'-GTTCCCATCGATGACATAG-3'); *Gapdh* was used as a reference gene with primers Gapdh-F and Gapdh-R.

For the endogenous A-2G mutant *SLC26A4* gene in the patients' PBMCs, the extent of FL transcript was calculated as a percentage of the total amount of two spliced transcripts. For minigenes and the chimeric gene in mouse tissues, the extent of the FL or exon 8-skipped isoform was calculated as a percentage of the total amount of three spliced transcripts.

Western blotting

Forty hours after transfection, HEK293 cells were harvested and lysed with MT-Cellytics protein extraction kit (Biocolors Bioscience, Shanghai, China). Protein samples were separated by 10% SDS-PAGE and transferred to nitrocellulose membranes (Pall Life Sciences, Port Washington, NY, USA). Blots were then incubated with primary monoclonal/polyclonal antibodies (mAbs/pAbs), followed by incubation with IRDye 680RD goat anti-mouse or anti-rabbit secondary antibody (LI-COR Biosciences, Lincoln, NE, USA). Anti-T7 mAb was a gift from Prof. Krainer at Cold Spring Harbor Laboratory, anti-GAPDH mAb was purchased from Santa Cruz Biotechnology (Dallas, TX, USA), anti-pendrin pAb was from Abcam (Waltham, MA, USA), and anti-hnRNP A1 pAb was from Proteintech (Wuhan, Hubei, China). Signals were detected by an Odyssey Infrared Imaging System (LI-COR Biosciences).

RNA-affinity chromatography

NE was purified from 500 μ L HEK293 cell pellet by ice-cold nuclear extraction buffer (20 mM HEPES [pH 7.9], 420 mM NaCl, 1.5 mM MgCl₂, 0.2 mM EDTA, 25% [v/v] glycerol, 0.5 mM DTT, and 0.5 mM PMSF).⁴² NE was then dialyzed against buffer D (20 mM

HEPES [pH 7.9], 100 mM KCl, 0.2 mM EDTA, 20% [v/v] glycerol, 0.5 mM DTT, and 0.5 mM PMSF) in a Slide-A-Lyzer dialysis cassette (Thermo Fisher Scientific) for 4 h at 4°C. Streptavidin agarose beads (Sigma-Aldrich) were pre-washed with buffer D for three times; 20 μ L was used to incubate with 2 nmol 5'-biotinylated WT RNA (5'-biotin-GUGUCCUCUUAGUAC-3') or mutant (5'-biotin-GUGUCCU CUUCGUAC-3') (Biosyntech) at 4°C for 2 h under rotation. RNA-bound beads were then rinsed with buffer D three times, followed by incubation with pre-cleared NE in buffer D and 0.2 U/mL RNase inhibitor (Beyotime Biotechnology, Shanghai, China) for 2 h at 4°C under rotation. At last, beads were washed three times with buffer D, and bound proteins were eluted with 1 \times Laemmli buffer and heated at 95°C for 10 min.

Statistical analysis

Data were analyzed by two-tailed Student's *t* test with the software SPSS 16.0 (IBM, Armonk, NY, USA) and presented as mean \pm standard deviation (SD). A *p* value <0.05 was considered statistically significant.

SUPPLEMENTAL INFORMATION

Supplemental information can be found online at <https://doi.org/10.1016/j.omtn.2022.03.015>.

ACKNOWLEDGMENTS

This work was supported by the National Natural Science Foundation of China (NSFC grants 82073753, 81530035, and 81471298 to Y.H.; NSFC grants 81822011 and 81771013 to Y.S.).

AUTHOR CONTRIBUTIONS

Y.H. and Y.S. designed the study. P.F., Z.X., J.C., M.L., Y.Z., D.W., and L.H. performed the experiments and analyzed data. Y.H., P.F., and L.W. wrote the manuscript. Y.H., Y.S., B.W., X.X., and D.L. contributed to the material support of the study. All authors have read and approved the final manuscript.

DECLARATION OF INTERESTS

A patent has been filed relating to the data presented. Y.H. is founder of ASOcura Pharmaceuticals (Suzhou).

REFERENCES

- Smith, R.J., Bale, J.F., Jr., and White, K.R. (2005). Sensorineural hearing loss in children. *Lancet* 365, 879–890.
- Cabanillas, R., Diñeiro, M., Cifuentes, G.A., Castillo, D., Pruneda, P.C., Alvarez, R., Sánchez-Durán, N., Capín, R., Plasencia, A., Viejo-Díaz, M., et al. (2018). Comprehensive genomic diagnosis of non-syndromic and syndromic hereditary hearing loss in Spanish patients. *BMC Med. Genom.* 11, 1–17.
- Everett, L.A., Glaser, B., Beck, J.C., Idol, J.R., Buchs, A., Heyman, M., Adawi, F., Hazani, E., Nassir, E., Baxevanis, A.D., et al. (1997). Pendred syndrome is caused by mutations in a putative sulphate transporter gene (PDS). *Nat. Genet.* 17, 411–422.
- Li, X.C., Everett, L.A., Lalwani, A.K., Desmukh, D., Friedman, T.B., Green, E.D., and Wilcox, E.R. (1998). A mutation in PDS causes non-syndromic recessive deafness. *Nat. Genet.* 18, 215–217.
- Scott, D.A., Wang, R., Kreman, T.M., Sheffield, V.C., and Karniski, L.P. (1999). The Pendred syndrome gene encodes a chloride-iodide transport protein. *Nat. Genet.* 21, 440–443.

6. Soleimani, M., Greeley, T., Petrovic, S., Wang, Z., Amlal, H., Kopp, P., and Burnham, C.E. (2001). Pendrin: an apical $\text{Cl}^-/\text{OH}^-/\text{HCO}_3^-$ exchanger in the kidney cortex. *Am. J. Physiol. Ren. Physiol.* 2800, F356–F364.
7. Pedemonte, N., Caci, E., Sondo, E., Caputo, A., Rhoden, K., Pfeffer, U., Di Candia, M., Bandettini, R., Ravazzolo, R., Zegarra-Moran, O., and Galletta, L.J. (2007). Thiocyanate transport in resting and IL-4-stimulated human bronchial epithelial cells: role of pendrin and anion channels. *J. Immunol.* 178, 5144–5153.
8. Choi, B.Y., Kim, H.M., Ito, T., Lee, K.Y., Li, X., Monahan, K., Wen, Y., Wilson, E., Kurima, K., Saunders, T.L., et al. (2011). Mouse model of enlarged vestibular aqueducts defines temporal requirement of *Slc26a4* expression for hearing acquisition. *J. Clin. Invest.* 121, 4516–4525.
9. Nakaya, K., Harbidge, D.G., Wangemann, P., Schultz, B.D., Green, E.D., Wall, S.M., and Marcus, D.C. (2007). Lack of pendrin HCO_3^- transport elevates vestibular endolymphatic $[\text{Ca}^{2+}]$ by inhibition of acid-sensitive TRPV5 and TRPV6 channels. *Am. J. Physiol. Ren. Physiol.* 292, F1314–F1321.
10. Wangemann, P., Nakaya, K., Wu, T., Maganti, R.J., Itza, E.M., Sanneman, J.D., Harbidge, D.G., Billings, S., and Marcus, D.C. (2007). Loss of cochlear HCO_3^- secretion causes deafness via endolymphatic acidification and inhibition of Ca^{2+} reabsorption in a Pendred syndrome mouse model. *Am. J. Physiol. Ren. Physiol.* 292, F1345–F1353.
11. Park, H.J., Shaikat, S., Liu, X.Z., Hahn, S.H., Naz, S., Ghosh, M., Kim, H.N., Moon, S.K., Abe, S., Tukamoto, K., et al. (2003). Origins and frequencies of *SLC26A4* (PDS) mutations in east and south Asians: global implications for the epidemiology of deafness. *J. Med. Genet.* 40, 242–248.
12. Wang, Q.J., Zhao, Y.L., Rao, S.Q., Guo, Y.F., Yuan, H., Zong, L., Guan, J., Xu, B.C., Wang, D.Y., Han, M.K., et al. (2007). A distinct spectrum of *SLC26A4* mutations in patients with enlarged vestibular aqueduct in China. *Clin. Genet.* 72, 245–254.
13. Dai, P., Li, Q., Huang, D., Yuan, Y., Kang, D., Miller, D.T., Shao, H., Zhu, Q., He, J., Yu, F., et al. (2008). *SLC26A4* c. 919-2A>G varies among Chinese ethnic groups as a cause of hearing loss. *Genet. Med.* 10, 586–592.
14. Yang, J.J., Tsai, C.C., Hsu, H.M., Shiao, J.Y., Su, C.C., and Li, S.Y. (2005). Hearing loss associated with enlarged vestibular aqueduct and Mondini dysplasia is caused by splice-site mutation in the PDS gene. *Hear. Res.* 199, 22–30.
15. Géléoc, G.S., and Holt, J.R. (2014). Sound strategies for hearing restoration. *Science* 344, 1241062.
16. Kim, M.A., Kim, S.H., Ryu, N., Ma, J.H., Kim, Y.R., Jung, J., Hsu, C.J., Choi, J.Y., Lee, K.Y., Wangemann, P., et al. (2019). Gene therapy for hereditary hearing loss by *SLC26A4* mutations in mice reveals distinct functional roles of pendrin in normal hearing. *Theranostics* 9, 7184–7199.
17. Juliano, R.L. (2016). The delivery of therapeutic oligonucleotides. *Nucleic Acids Res.* 44, 6518–6548.
18. Stein, C.A., and Castanotto, D. (2017). FDA-approved oligonucleotide therapies in 2017. *Mol. Ther.* 25, 1069–1075.
19. Hua, Y., Sahashi, K., Rigo, F., Hung, G., Horev, G., Bennett, C.F., and Krainer, A.R. (2011). Peripheral SMN restoration is essential for long-term rescue of a severe spinal muscular atrophy mouse model. *Nature* 478, 123–126.
20. Wadman, M. (2016). Antisense rescues babies from killer disease. *Science* 354, 1359–1360.
21. Lentz, J., Savas, S., Ng, S.S., Athas, G., Deininger, P., and Keats, B. (2005). The *USH1C* 216G→A splice-site mutation results in a 35-base-pair deletion. *Hum. Genet.* 116, 225–227.
22. Lentz, J.J., Jodelka, F.M., Hinrich, A.J., McCaffrey, K.E., Farris, H.E., Spalitta, M.J., Bazan, N.G., Duelli, D.M., Rigo, F., and Hastings, M.L. (2013). Rescue of hearing and vestibular function by antisense oligonucleotides in a mouse model of human deafness. *Nat. Med.* 19, 345–350.
23. Lentz, J.J., Pan, B., Ponnath, A., Tran, C.M., Nist-Lund, C., Galvin, A., Goldberg, H., Robillard, K.N., Jodelka, F.M., Farris, H.E., et al. (2020). Direct delivery of antisense oligonucleotides to the middle and inner ear improves hearing and balance in Usher mice. *Mol. Ther.* 28, 2662–2676.
24. Parada, G.E., Munita, R., Cerda, C.A., and Gysling, K. (2014). A comprehensive survey of non-canonical splice sites in the human transcriptome. *Nucleic Acids Res.* 42, 10564–10578.
25. Lee, H.J., Jung, J., Shin, J.W., Song, M.H., Kim, S.H., Lee, J.H., Lee, K.A., Shin, S., Kim, U.K., Bok, J., et al. (2014). Correlation between genotype and phenotype in patients with bi-allelic *SLC26A4* mutations. *Clin. Genet.* 86, 270–275.
26. Sun, J., Bai, J., Jiang, T., Gao, Y., and Hua, Y. (2019). Modulation of *PDCD1* exon 3 splicing. *RNA Biol.* 16, 1794–1805.
27. Geuens, T., Bouhy, D., and Timmerman, V. (2016). The hnRNP family: insights into their role in health and disease. *Hum. Genet.* 135, 851–867.
28. Burd, C.G., and Dreyfuss, G. (1994). RNA binding specificity of hnRNP A1: significance of hnRNP A1 high-affinity binding sites in pre-mRNA splicing. *EMBO J.* 13, 1197–1204.
29. Cartegni, L., Hastings, M.L., Calarco, J.A., De Stanchina, E., and Krainer, A.R. (2006). Determinants of exon 7 splicing in the spinal muscular atrophy genes, *SMN1* and *SMN2*. *Am. J. Hum. Genet.* 78, 63–77.
30. Wu, X., Wang, S.H., Sun, J., Krainer, A.R., Hua, Y., and Prior, T.W. (2017). A-44G transition in *SMN2* intron 6 protects patients with spinal muscular atrophy. *Hum. Mol. Genet.* 26, 2768–2780.
31. Li, X., Sanneman, J.D., Harbidge, D.G., Zhou, F., Ito, T., Nelson, R., Picard, N., Chambrey, R., Eladari, D., Miesner, T., et al. (2013). *SLC26A4* targeted to the endolymphatic sac rescues hearing and balance in *Slc26a4* mutant mice. *Plos Genet.* 9, e1003641.
32. Miyagawa, M., Nishio, S., and Usami, S. (2014). Mutation spectrum and genotype-phenotype correlation of hearing loss patients caused by *SLC26A4* mutations in the Japanese: a large cohort study. *J. Hum. Genet.* 59, 262–268.
33. Hua, Y., Vickers, T.A., Okunola, H.L., Bennett, C.F., and Krainer, A.R. (2008). Antisense masking of an hnRNP A1/A2 intronic splicing silencer corrects *SMN2* splicing in transgenic mice. *Am. J. Hum. Genet.* 82, 834–848.
34. Xing, M., Tokumar, Y., Wu, G., Westra, W.B., Ladenson, P.W., and Sidransky, D. (2003). Hypermethylation of the Pendred syndrome gene *SLC26A4* is an early event in thyroid tumorigenesis. *Cancer Res.* 63, 2312–2315.
35. Hammond, S.M., Aartsma-Rus, A., Alves, S., Borgos, S.E., Buijssen, R.A.M., Collin, R.W.J., Covello, G., Denti, M.A., Desviat, L.R., Echevarria, L., et al. (2021). Delivery of oligonucleotide-based therapeutics: challenges and opportunities. *EMBO Mol. Med.* 13, e13243.
36. Stenson, P.D., Mort, M., Ball, E.V., Evans, K., Hayden, M., Heywood, S., Hussain, M., Phillips, A.D., and Cooper, D.N. (2017). The Human Gene Mutation Database: towards a comprehensive repository of inherited mutation data for medical research, genetic diagnosis and next-generation sequencing studies. *Hum. Genet.* 136, 665–677.
37. Lord, J., Gallone, G., Short, P.J., McRae, J.F., Ironfield, H., Wynn, E.H., Gerety, S.S., He, L., Kerr, B., Johnson, D.S., et al. (2019). Deciphering Developmental Disorders study. Pathogenicity and selective constraint on variation near splice sites. *Genome Res.* 29, 159–170.
38. Bruun, G.H., Bang, J.M.V., Christensen, L.L., Brøner, S., Petersen, U.S.S., Guerra, B., Grønning, A.G.B., Doktor, T.K., and Andresen, B.S. (2018). Blocking of an intronic splicing silencer completely rescues *IKBKAP* exon 20 splicing in familial dysautonomia patient cells. *Nucleic Acids Res.* 46, 7938–7952.
39. Grønning, A.G.B., Doktor, T.K., Larsen, S.J., Petersen, U.S.S., Holm, L.L., Bruun, G.H., Hansen, M.B., Hartung, A.M., Baumbach, J., and Andresen, B.S. (2020). DeepCLIP: predicting the effect of mutations on protein-RNA binding with deep learning. *Nucleic Acids Res.* 48, 7099–7118.
40. Sinha, R., Kim, Y.J., Nomakuchi, T., Sahashi, K., Hua, Y., Rigo, F., Bennett, C.F., and Krainer, A.R. (2018). Antisense oligonucleotides correct the familial dysautonomia splicing defect in *IKBKAP* transgenic mice. *Nucleic Acids Res.* 46, 4833–4844.
41. Li, M.Z., and Elledge, S.J. (2007). Harnessing homologous recombination *in vitro* to generate recombinant DNA via SLIC. *Nat. Methods* 4, 251–256.
42. Carey, M.F., Peterson, C.L., and Smale, S.T. (2009). Dignam and Roeder nuclear extract preparation. *Cold Spring Harb. Protoc.* 2009, pdb.prot5330.